PAPER

Improved coalescence stability of monodisperse phospholipid-coated microbubbles formed by flow-focusing at elevated temperatures

Tim Segers, [iD]* Anne Lassus, Philippe Bussat, Emmanuel Gaud and Peter Frinking

Monodisperse phospholipid-coated ultrasound contrast agent (UCA) microbubbles can be directly synthesized in a lab-on-a-chip flow-focusing device. However, high total lipid concentrations are required to minimize on-chip bubble coalescence. Here, we characterize the coalescence probability and the long-term size stability of microbubbles formed using DPPC and DSPC based lipid mixtures as a function of temperature. We show that the coalescence probability can be dramatically reduced by increasing the temperature during bubble formation. Moreover, it is shown that the increased coalescence stability can be explained from an exponential increase of the relative viscosity in the thin liquid film between the colliding bubbles. Furthermore, it was found that the relative viscosity of a DPPC lipid mixture is 7.6 times higher than that of a DSPC mixture and that it can be explained solely from the higher DPPC liposome concentration. Regarding long-term bubble stability, the ratio of the initial on-chip bubble size to the final stable bubble size was always found to be 2.2 for DPPC and DSPC coated bubbles with 10 mol% DPPE-PEG5000, independent of the temperature. Moreover, it was demonstrated that the microbubble suspensions formed at elevated temperatures are highly stable over a time window of 2 to 4 days when collected in a vial. All in all, this work shows that, by increasing the temperature during bubble formation from room temperature to 70 °C, the efficiency of the use of phospholipids in microbubble formation by flow-focusing can be increased by 5 times.

1 Introduction

Ultrasound contrast agents (UCA) typically consist of a suspension of phospholipid-coated microbubbles with radii ranging from 0.5 to 5 μm. Upon exposure to ultrasound, the microbubbles oscillate thereby generating harmonic echoes that allow for the visualization and quantification of organ perfusion.[1,2] The acoustic response of a microbubble is strongly dependent on the coupling between the ultrasound driving frequency and the microbubble resonance frequency, the latter being inversely proportional to the microbubble size.[3] Clinical ultrasound scanners typically operate over a narrow frequency bandwidth, relative to the resonance frequencies of the microbubbles present in a typical UCA. Thus, only a small fraction of the UCA population contributes to the overall echo. Therefore, the sensitivity of contrast enhanced ultrasound imaging, and in particular that of molecular imaging,[4] can be increased by 2 to 3 orders of magnitude through the use of monodisperse bubbles that are resonant to the driving ultrasound pulse.[5] Moreover, the delivery of drugs and genetic material (*e.g.*, mRNAs or siRNAs) to target cells

using functionalized microbubbles and ultrasound[6–10] is expected to be more efficient and more precise using a suspension of monodisperse bubbles due to its uniform acoustic response.[11]

Monodisperse bubble suspensions can be obtained through decantation,[12] mechanical filtration,[13] and centrifugation[14] of a polydisperse agent. Polydisperse bubbles can be sorted in microfluidic devices at a higher precision, *e.g.* microbubbles can be sorted to size in a pinched microchannel[15] and they can be sorted to their acoustic response using the primary radiation force.[16] Monodisperse microbubbles can also be produced directly using a lab-on-a-chip based microfluidic flow-focusing device. In a flow-focusing device a gas thread is focused between two liquid flows through an orifice where the gas thread destabilizes due to capillary instability and pinches off to release monodisperse bubbles, see Fig. 1A.[17–22]

The use of flow-focusing methods for the synthesis of stable monodisperse phospholipid-coated microbubbles is non-trivial.[23–25] Freshly formed phospholipid-coated microbubbles formed by flow-focusing are inherently unstable, prone to Ostwald ripening, and they always decrease in size during their stabilization.[26,27] The diffusive dissolution mechanically compresses the lipid monolayer, thereby

Bracco Suisse S.A., Route de la Galaise 31, 1228 Geneva, Switzerland.
E-mail: t.j.segers@utwente.nl
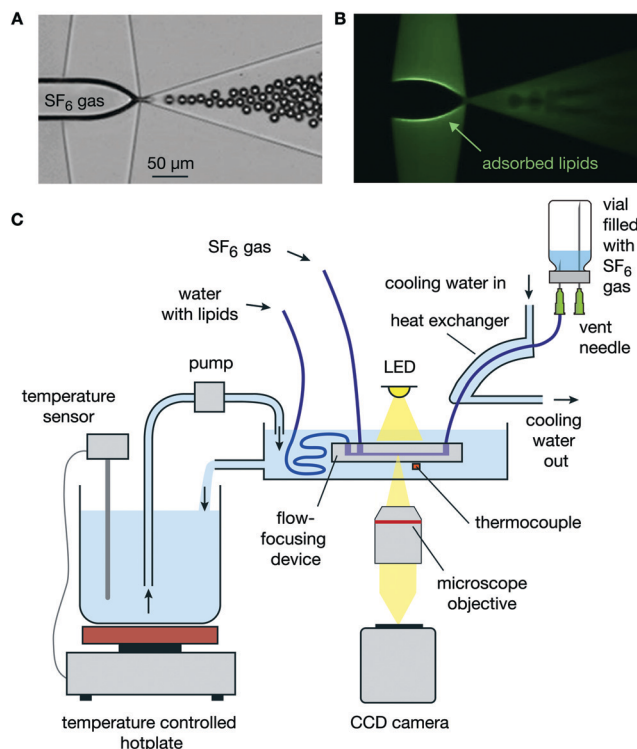
Fig. 1 (A) Bright-field image of the flow-focusing device used in this study. (B) Fluorescence image of the flow-focusing device showing a high fluorescent intensity from lipids adsorbed to the gas–liquid interface. A fluorescent probe was chemically attached to the DPPE-PEG5000 lipids. (C) The temperature at which the microbubbles were formed was controlled using a thermostatic bath in which the flow-focusing device was immersed. Water was pumped from a temperature controlled beaker on a hot-plate to the thermostatic bath. The formed bubbles were cooled down to room temperature after their formation using a heat exchanger.

increasing its surface pressure and decreasing the Laplace pressure-driven dissolution. Moreover, the mechanical compression results in a barrier for the gas molecules due to the closely packed lipid molecules. During the stabilization process, the total number of lipid molecules in the bubble shell remains unchanged.[26] For bubbles formed at room temperature using a mixture of DPPC, DPPA, and DPPE-PEG5000, the ratio of the initial bubble radius R_i to the final stable bubble radius R_f increases with PEG molecular weight M_w, PEG molar fraction ϕ_{PEG}, and the propylene glycol mass fraction λ_{PG} as follows: $R_i R_f^{-1} = 1.4 + \alpha(1 + \gamma \lambda_{PG}^2) M_w \phi_{PEG}$ where $\alpha = 1.6 \times 10^{-3}$ mol g^{-1} and $\gamma = 30$.[27] Thus, the bubble size decrease during stabilization originates from both, the primary lipids (factor of 1.4) and the PEGylated lipid. Primary phospholipids are thermodynamically active, *i.e.* they have a phase transition temperature at which the mobility of the lipids dramatically increases from a solid-like state to a liquid-like behavior.[28] Furthermore, the conformation of a PEG chain in an aqueous medium is temperature dependent, *i.e.* it collapses at increased temperatures.[29] However, the stabilization process of microbubbles coated by a mixture of primary and PEGylated phospholipids formed by flow-focusing as a function of the bubble formation temperature has never been studied.

A second complicating factor of flow-focusing methods for the synthesis of monodisperse phospholipid-coated microbubbles is microbubble coalescence in the outlet of the flow-focusing device, particularly at high production rates. Coalescence of the freshly formed microbubbles results in a lower bubble concentration and in a broader microbubble size distribution, both resulting in a lower amount of bubbles resonant to the ultrasound transmit frequency and thus, in a less efficient contrast agent. Moreover, coalescence of monodisperse bubbles with a uniform acoustic response[11] results in a polydisperse bubble suspension with a nonuniform acoustic response and thereby in a contrast agent with a decreased potential for molecular- and deep tissue imaging.[5] For all these reasons, coalescence should be minimized. At the high lipid concentrations required to minimize bubble coalescence, the efficiency of the phospholipid coating process is low. Typically, less than 0.1% of the total lipid concentration is adsorbed to the microbubble shell, while even at concentrations one order of magnitude lower, the gas–liquid interface is already fully saturated with lipids[26,27] (see also Fig. 1B). Recently, it has been shown that the high concentration of free PEGylated liposomes inhibits coalescence through an effective increase of the relative viscosity Φ_r in the thin film between colliding bubbles.[27] In the same paper, a universal power law for Φ_r has been developed: $\Phi_r = 1 + Kc_\infty^2 \phi_{PEG}^3 M_w^4 \eta_0^{-1}$, with c_∞ the total lipid concentration, η_0 the bulk viscosity, and K a constant. Moreover, it has been shown that this universal equation for Φ_r together with the coalescence model for microbubbles in the outlet of a flow-focusing device:[27]

$$P \simeq \exp\left[-\Phi_r \beta \frac{R}{H} \frac{Q_t}{Q_g}\right], \qquad (1)$$

have predictive power, in a way that the phospholipid formulation can be designed such that the coalescence probability P is minimized for any given gas flow-rate Q_g, total flow-rate Q_t, bubble radius R, and microfluidic channel height H ($\beta = 0.024$).

The increase of the relative viscosity Φ_r in the thin liquid film between colliding bubbles results from the mutual interaction between the PEGylated liposomes and between the liposomes and the PEGylated microbubble surface through surface- and colloidal forces.[27,30] Rheology is typically temperature dependent.[31] Moreover, surface- and colloidal forces, *e.g.* steric interactions and the structural force, are reported to increase with an increase in temperature.[30,32] Therefore, Φ_r is expected to be temperature dependent thereby potentially allowing for an increased efficiency of the use of the phospholipids at temperatures exceeding room temperature. Here, microbubble coalescence in the outlet of a lab-on-a-chip flow-focusing device was characterized at temperatures ranging from 15 °C up to 70 °C in order to extend

the universal equation for Φ_r with its temperature dependence. Furthermore, the effect of the bubble formation temperature on microbubble stabilization and long-term size- and concentration stability was measured for DPPC and DSPC based lipid mixtures.

2 Materials and methods

2.1 Phospholipid formulations

Two different phospholipid mixtures were studied. The first one consisted primarily of DPPC that was mixed with DPPA and DPPE-PEG5000 at a molar ratio of $8:1:1$, respectively. The total lipid concentration was 2.0 mmol L^{-1} (2.5 mg mL^{-1}). The second mixture consisted of DSPC mixed with DPPA and DPPE-PEG5000 also at a molar ratio of $8:1:1$, respectively, and at a total lipid concentration of 3.9 mmol L^{-1} (5.0 mg mL^{-1}). The concentration of the DSPC mixture was deliberately chosen twice that of the DPPC mixture since coalescence was more severe for the DSPC based mixture. The lipids were dispersed in phosphate buffered saline (PBS) and they were prepared exactly as described in detail by Segers et al.[27] No co-solvents or viscosity increasing chemicals, e.g. propylene glycol and glycerol, were added as they are known to degrade the monodispersity and the stability of the final bubble suspension.[27] After sonication of the lipid dispersion, a Zetasizer (Malvern, ZetaSizer, Nano ZSP) was used to measure the liposome size distributions; 10 μL of the concentrated lipid dispersion was diluted in 1 mL of PBS before the measurement.

2.1.1 Flow-focusing device.
The employed flow-focusing device is shown in Fig. 1A. It had a nozzle width of 5 μm that expanded into a 500 μm wide outlet channel at a 17.5° angle. The overall channel height H was 14 μm. The chip was fabricated in PDMS using standard soft lithography techniques[33] as described before.[27] The liquid flow rate was controlled via a syringe pump (Harvard Apparatus, PHD 4400, Holliston, MA), and the gas pressure (SF_6, Air Liquide Healthcare, Plumsteadville, PA) was controlled using a pressure regulator (PRG101-25, Omega). For both lipid mixtures, the liquid flow-rate ranged from 10 to 40 μL min^{-1} and the gas pressure ranged from 60 to 100 kPa gauge.

2.1.2 Temperature control.
To control the temperature during bubble formation, the flow-focusing device was immersed in a $15 \times 10 \times 4$ cm^3 ($l \times b \times h$) thermostatic water bath, see Fig. 1C. Temperature controlled water was pumped at an approximate flow-rate of 0.2 L min^{-1} from a 1 L glass beaker, positioned on a temperature controlled hot plate (IKA RET basic and IKA ETS-D5, Sigma-Aldrich), into the water bath containing the flow-focusing device. The excess water in the bath drained by gravity back to the 1 L beaker keeping the water level constant. To verify that the temperature was stable within ±0.5 °C during the measurements, the temperature at the location of the flow-focusing device was measured using a thermocouple connected to a thermometer (HH1470U, data logger thermometer, Omega). The liquid inlet tubing (PEEK, Upchurch) of the flow-focusing device was

immersed in the temperature controlled water bath over approx. 10 cm before entering the chip to allow the temperature of the lipid dispersion to equilibrate with that of the thermostatic bath.

2.2 Cooling of the formed microbubbles

The outlet port of the flow-focusing device was connected to 0.5 mm inner diameter outlet tubing that was passed through 5 mm inner diameter silicone tubing over a length of 10 cm. Water at room temperature was pumped through the 5 mm silicone tubing to cool the freshly formed bubbles. The time between bubble formation and cooling was 200 ms during all experiments except for one additional experiment where the freshly formed bubbles, produced at 50 °C, were cooled down 200 ms, 1.5 min, and 3 min after their formation to investigate the importance of cooling. To this end, the length of the outlet tubing within the thermostatic bath was controlled such that the time between bubble formation and subsequent cooling was varied. The bubbles were collected for 5 min in a vial of which the headspace was filled with SF_6 gas, see Fig. 1C. The size distributions of the bubble samples were measured using a coulter counter (Multisizer 3, 30 μm aperture tube, Beckman Coulter, Brea, CA, USA) 1 h after bubble production to allow the bubbles to stabilize to their final size.

2.2.1 Imaging setup.
The water bath containing the flow-focusing device was placed on an inverted microscope (Olympus IX50) coupled to a CCD camera (Lumenera, LM165M, pixelsize: 6.45×6.45 μm^2) and a 10×, a 20×, and a 40× magnifying objective (Olympus LCPlanFl). Illumination was provided by a high-intensity LED (Everlight, EHP-C52C) that produced a single 300 ns flash per imaging frame.

2.2.2 Coalescence and stability measurement.
First, the temperature was set and the thermometer was used to verify that the water had reached thermal equilibrium. Then, the flow-rate and gas pressure were set and bubbles were produced for 5 min such that the outlet tube was fully filled with microbubbles formed under the same conditions. Subsequently, 100 images of the nozzle region (Fig. 2C and D) were captured to measure the initial radius R_i of the freshly formed bubbles. Afterwards, a second set of 100 images was captured of the full width of the 500 μm wide rectangular outlet channel to measure the coalescence percentage. Finally, the bubble suspension at the outlet tube was pipetted and transferred to one of the ten $7.0 \times 4.0 \times 0.1$ mm^3 compartments of a flow cell that was fabricated using double-sided tape (3M Scotch, 665 Permanent) and two microscope slides. Bubble formation was measured at ten different flow rates to cover the minimum and maximum possible coalescence percentage. After the 10 repeated measurements, and after an additional stabilization time of 30 min, 100 microscope images were captured from different areas of each of the 10 flow-cell compartments to measure the final bubble radius R_f. A complete measurement series at a constant temperature consisted of 10 initial bubble radius measurements,
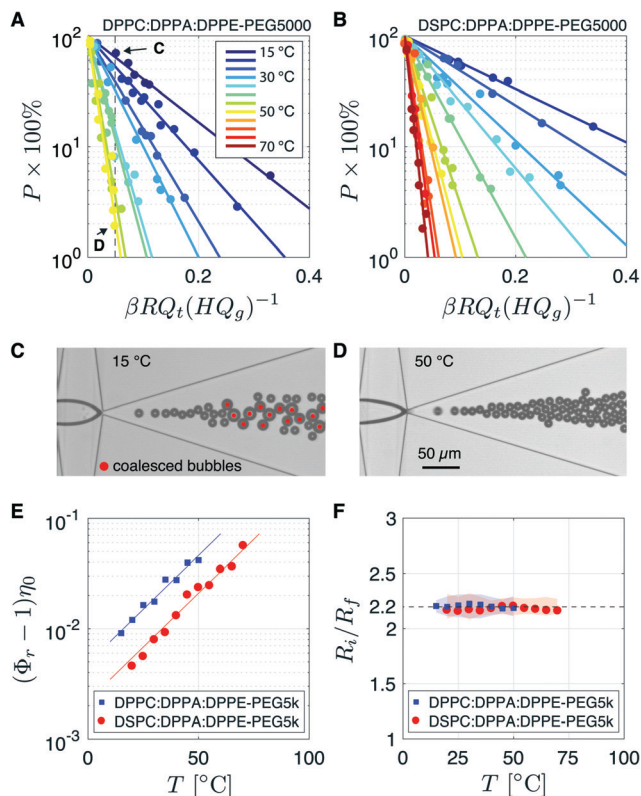
Fig. 2 (A) Percentage of coalesced bubbles measured for the DPPC lipid mixture at temperatures ranging from 15 °C to 50 °C. (B) Percentage of coalesced bubbles for the DSPC lipid mixture measured at temperatures ranging from 20 °C to 70 °C. (C) The percentage of coalesced bubbles produced at $\beta R Q_t (H Q_g)^{-1} = 0.05$ was 70% while that at (D) 50 °C was only 2%. (E) $(\Phi_r - 1)\eta_0$ as a function of the temperature of bubble formation for the DPPC and the DSPC lipid mixtures. (F) Ratio of the initial on-chip bubble radius R_i to the final stable bubble radius R_f as a function of the temperature at which the bubbles were synthesized.

10 coalescence percentages, and 10 final bubble size measurements. After a completed series of experiments, the temperature was changed and the measurement series was repeated.

2.2.3 Image processing. The image series were processed in MATLAB (The Mathworks, Natick, MA) to find the initial bubble size distribution, the final bubble size distribution, and the size distribution in the rectangular outlet channel of the flow-focusing device. All details regarding the image processing method can be found in.[27] From the bubble size distribution measured in the rectangular 14×500 μm² outlet channel of the flow-focusing device, the coalescence probability was calculated as follows:

$$P = \frac{\sum_2^n n N_n}{N_{tot}}, \tag{2}$$

where n is the number of the n-th peak in the size distribution, N_n the number of bubbles within the nth peak, and N_{tot} the total number of bubbles: $N_{tot} = \sum_2^n n N_n$.

The gas flow-rate Q_g was calculated as follows:

$$Q_g = \frac{N_{tot} V_B Q_l}{2 T F_L H - N_{tot} V_B}, \tag{3}$$

where V_B is the volume of the initially formed bubble $V_B = 4/3 \pi R_i^3$, $N_{tot} V_B$ the total amount of gas per image, $2 T F_L H$ the total volume of the outlet channel within the image with F_L the length of the imaged part of the rectangular outlet channel having a width of $2T = 500$ μm and a height of $H = 14$ μm.

2.2.4 Microbubble stability in the collection vial as a function of the bubble formation temperature. The effect of temperature during bubble formation on the long-term size- and concentration stability of bubble suspensions formed at temperatures of 25 °C, 45 °C, 55 °C, and 65 °C was measured. The microbubbles were produced at a liquid flow-rate of 35 μL min⁻¹ using the DSPC based lipid mixture. The gas pressure was set such that bubbles with an on-chip radius of 7.0 ± 0.3 μm were formed. The formed bubbles were collected in a vial that was sealed by a rubber stopper and filled with SF₆ gas before bubble collection, see Fig. 1C. During bubble collection, the outlet of the flow-focusing device was connected to a 24G needle. The needle was pierced just through the rubber stopper. A vent needle, also pierced through the rubber stopper, was positioned against the bottom of the glass vial that was placed upside-down during bubble collection. Since SF₆ gas has a higher density than air, it does not spontaneously drain from the vial and it therefore allows the bubbles to stabilize in a SF₆ gas environment. Note that when the SF₆-filled bubbles would be collected in an air-filled vial, the gas concentration difference would drive air into the bubbles and SF₆ out, thereby decreasing microbubble stability. Bubbles were collected for 15 minutes after which the needles were removed. The vial was put to rest to allow the bubbles to stabilize and the size distributions were measured 2 hours and 2 days after bubble formation using a coulter counter.

2.3 Long-term stability in the vial: DPPC *versus* DSPC coated bubbles

In the final experiment, the long-term stability of a microbubble suspension formed using the DPPC based lipid mixture and collected in a vial was characterized and compared to that of a bubble suspension formed using the DSPC based lipid mixture. The bubbles were produced at a temperature of 60 °C and at a liquid flow-rate of 35 μL min⁻¹. The bubbles were collected for 15 min as before, in a vial with a SF₆ gas headspace. The size distributions were measured 2 hours, 2 days, 4 days, and 7 days after bubble collection using a coulter counter.

3 Results and discussion

3.1 Temperature dependent microbubble coalescence

Fig. 2A shows the percentage of coalesced bubbles, formed using the DPPC based lipid mixture, as a function of the

dimensionless parameter $\beta RQ_t(HQ_g)^{-1}$ (see eqn (1)) for temperatures ranging from 15 °C up to 50 °C. For the DSPC based lipid mixture the percentage of coalesced bubbles is plotted in Fig. 2B for temperatures ranging from 20 °C up to 70 °C. Note that for both lipid formulations the coalescence probability of bubbles formed at the same dimensionless value $\beta RQ_t(HQ_g)^{-1}$ decreases with increasing temperature. To illustrate the dramatic effect of temperature on the bubble coalescence probability, Fig. 2C and D show images of the expanding nozzle of the flow-focusing device for $\beta RQ_t(HQ_g)^{-1} = 0.05$ at temperatures of 15 °C and 50 °C, respectively. The percentage of coalesced bubbles at 15 °C (Fig. 2C) was 70%, while at 50 °C (Fig. 2D) it was only 2% (see data points indicated by C and D in Fig. 2A). Thus, the coalescence probability of phospholipid coated monodisperse microbubbles produced by flow-focusing can be dramatically reduced by increasing the temperature during bubble formation.

The relative viscosity Φ_r was obtained by fitting an exponential function ($y = \exp(-ax) \times 100\%$) to the data points per temperature (see solid lines in Fig. 2A and B). To investigate the contribution of the phospholipids to Φ_r, $(\Phi_r - 1)\eta_0$ is plotted in Fig. 2E as a function of temperature. The temperature dependence of η_0 was calculated using $\eta_0(T) = A \times 10^{B/(T-C)}$, where $A = 2.414 \times 10^{-5}$ Pa s, $B = 247.8$ K, and $C = 140$ K.[34] The data points collapse on two parallel exponential curves showing that $(\Phi_r - 1)\eta_0 \propto \exp(kT)$, where $k = 0.047$ K^{-1}. Note that, even though the total lipid concentration of the DSPC mixture was 2 times higher than that of the DPPC mixture, Φ_r of the DSPC mixture is 2 times lower than that of the DPPC mixture. Thus, since $\Phi_r \propto c_\infty^2$,[27] at an equal total lipid concentration and for a given temperature, Φ_r of the DPPC lipid mixture is 7.6 times higher than that of the DSPC lipid mixture.

To investigate the origin of the 7.6 times higher Φ_r of the DPPC lipid mixture with respect to that of the DSPC mixture, the liposome size distributions are plotted in Fig. 3. Note that the liposome size only slightly increases when the temperature is increased from 25 °C to 60 °C. Also note that the DSPC liposomes are on average 2.8 times larger than the DPPC liposomes whereas the area per lipid molecule is approximately the same for DSPC and DPPC molecules.[35,36] The liposome concentration is inversely proportional to the bi-

layer surface area per liposome. Thus, the liposome concentration of the DPPC lipid mixture is 7.8 times higher than that of the DSPC lipid mixture which is in excellent agreement with the 7.6 higher Φ_r of the DPPC based lipid mixture suggesting that the higher Φ_r results purely from the higher liposome concentration and not from the difference in the employed primary phospholipid. Future work may investigate the role of liposome size on coalescence stability in more detail using, *e.g.*, extrusion methods.[37] The liposomes formed through sonication of the DPPC and DSPC lipid mixtures are fully covered with surface grafted PEG5000 brushes.[38] The PEG brushes shield the DPPC and DSPC molecules from the subphase which explains that Φ_r is independent of the employed primary phospholipid molecule.

Using the experimentally obtained scaling of the relative viscosity Φ_r with temperature, the universal equation for Φ_r obtained in our previous work[27] is extended with the temperature dependence, as follows:

$$\Phi_r(T) = 1 + \frac{c_\infty^2 \phi_{PEG}^3 M_w^4}{\eta_0(T)} \Omega e^{kT}, \qquad (4)$$

with T the absolute temperature in Kelvin, c_∞ the total lipid concentration in mol m^{-3}, and $k = 0.047$ K^{-1}. The constant $\Omega = 5.024 \times 10^{-17}$ mol^2 m^5 kg^{-3} s^{-1} for the DPPC based formulation. To calculate Φ_r for a DSPC based formulation, Ω should simply be divided by a factor of 7.6. Fig. 4 shows all coalescence probability data measured in this work, and in our previous work.[27] All data collapse on a single master curve. Thus, the percentage of bubbles that will coalesce in the outlet of a flow-focusing device can be predicted for DPPC and for DSPC based formulations using eqn (1) and (4).

Monodisperse bubbles can be produced at high production rates and at room temperature for DPPC based lipid formulations at a total lipid concentration on the order of 10 mg mL^{-1}.[26] However, for a DSPC based formulation with the same molar PEG ratio, Φ_r is 7.6 times lower. Therefore, the total lipid concentration of the DSPC formulation needs to be 2.8 times higher than that of the DPPC formulation in order
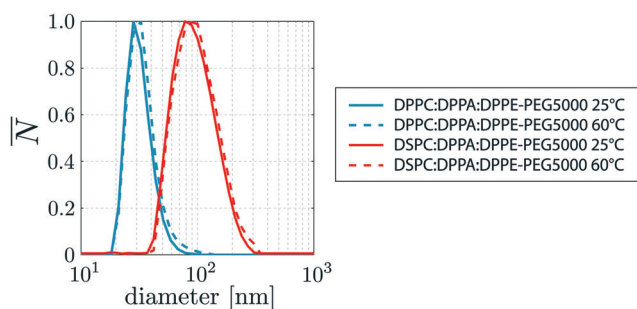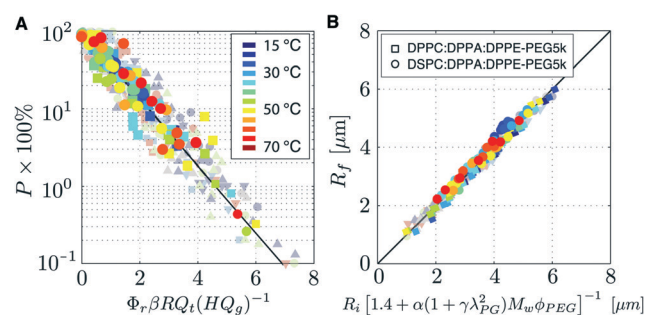

Fig. 3 Liposome size distributions of the DPPC and DSPC based lipid formulations studied in this work measured at a temperature of 25 °C and 60 °C.

Fig. 4 (A) Master plot of the temperature dependent coalescence probability data and (B) of the stabilization data measured for the DPPC:DPPA:DPPE-PEG5000 lipid mixture (squares) and for the DSPC:DPPA:DPPE-PEG5000 lipid mixture (circles). Transparent data points are reproduced from our previous work.[27]

to produce monodisperse bubbles at room temperature at the same coalescence probability. However, by increasing the temperature from room temperature to 50 °C, eqn (4) shows that the coalescence probability of the DSPC formulation can be lowered such that it is equal to that of the DPPC based formulation used at room temperature. More generally speaking, eqn (4) shows that for any lipid formulation used under certain flow conditions resulting in coalescence probability P, a 5 times lower lipid concentration c_∞ results in the very same coalescence probability when the temperature is increased from room temperature to 70 °C. Thus, the use of phospholipids in microbubble formation by flow-focusing becomes 5 times more efficient by increasing the bubble formation temperature from room temperature to 70 °C.

Eqn (4) can also be written in terms of the liposome concentration. However, to allow the equations to be used in practice, where liposome concentration measurements require specialized equipment, it was decided to write eqn (4) in terms of the parameters controlled in the lab, i.e. c_∞, ϕ_{PEG}, and M_w.

To date, to the best of the author's knowledge, no temperature dependent rheological data is available on an aqueous dispersion of PEGylated liposomes in an extensional flow such as that found in the thin film between colliding bubbles. Nevertheless, it may be speculated that the exponential scaling of Φ_r with T results from the steric interaction between the liposomes and the monomolecular film around the bubbles. However, in principle the steric interaction force scales linearly with T,[28,30] which is very different from the exponential dependence as observed here. Modeling the full temperature dependent liposome–monolayer and liposome–liposome interactions during the drainage of a thin film, by Monte Carlo[39] or molecular dynamics[40] simulations, may reveal the underlying physics of the observed scaling.

Here, it was demonstrated that the efficiency of the use of surfactants increases with temperature. This may not only be important for the synthesis of bubbles in lab-on-a-chip based devices but also for the stable formation of droplets, e.g. for the formation of phase-change agents.[41]

3.2 Temperature dependent microbubble stabilization

The bubbles that were formed at the different temperatures and flow conditions were left to stabilize in the flow cell. The ratio of the initial bubble radius R_i to the final stable bubble radius R_f was obtained by fitting a linear function to the data per temperature, see Fig. 2F. The root-mean-square (RMS) of the fitting residuals is represented by the shaded areas. A unique temperature independent relation is found between R_i and R_f where the final bubble size is always found to be 2.2 times smaller than the initial bubble size. The ratio $R_i/R_f = 2.2$ is exactly as that predicted by the universal equation for the ratio of the initial bubble radius R_i to the final bubble radius that was obtained in our previous work:[27]

$$\frac{R_i}{R_f} = 1.4 + \alpha\left(1 + \gamma\lambda_{PG}^2\right)M_w\phi_{PEG} \qquad (5)$$

where $\alpha = 1.6 \times 10^{-3}$ mol g^{-1}, $\gamma = 30$, and λ_{PG} the propylene glycol mass fraction. All stabilization data obtained in this work, and in our previous work,[27] are plotted in Fig. 4B rescaled according to eqn (5). All data collapse on a single master curve. Thus, for DPPC and DSPC based formulations with 10 mol% of DPPE-PEG5000, eqn (5) predicts the final bubble size for a given initial on-chip bubble size. Moreover, here, we found that the ratio R_i/R_f is independent of the bubble formation temperature.

From Langmuir trough surface pressure-area isotherms, it is well known that at a constant surface pressure, the area per lipid molecule increases with temperature.[35] The increase in surface area per lipid molecule in the bubble shell of a freshly formed bubble synthesized at a temperature higher than room temperature would lead to an increased ratio of R_i/R_f with respect to that of a bubble formed at room temperature, since R_f of both bubbles is measured at the same temperature, i.e. at room temperature. However, here, we surprisingly found a constant temperature independent ratio of R_i/R_f. This may be explained from the collapse of the PEG chain at elevated temperatures. The state of the PEG chain depends on the affinity of the polymer with the medium. In a poor solvent, a PEG chain collapses and in a good solvent it swells; increasing its excluded volume to above that of a PEG chain conformed as a Gaussian coil in pure water.[29,38] An increase in temperature decreases the affinity of the PEG chain with water and thereby its excluded volume. This may cancel out the increase in the area per primary lipid molecule. Nevertheless, to confirm this hypothesis further quantification of the ratio of R_i/R_f is required for bubbles coated with a range of PEG molar ratios.

Even though a constant ratio of R_i/R_f was found here, the conformation, that is, the microstructure of the monomolecular microbubble shell may be different for microbubbles formed at different temperatures.[42] The conformation of the microbubble shell may play a role in the acoustic response of the microbubble to an ultrasound driving pulse. Therefore, further research towards acoustic characterization of microbubbles formed at different temperatures would be valuable.

In this study, SF$_6$ gas was used as microbubble filling gas. In our previous studies we used C$_4$F$_{10}$ and air to fill the microbubbles. For all filling gasses exactly the same ratio between the initial bubble size and the final stable bubble size has been found.[26,27] Thus, this confirms once more that the ratio of R_i/R_f of phospholipid-coated microbubbles formed by flow-focusing is independent of the filling gas.[26,27] Nevertheless, the lower the aqueous solubility and diffusivity of the microbubble filling gas in water, the longer the time window of the diffusive stabilization process of the freshly formed microbubbles.

3.2.1 Cooling the formed microbubbles: effect on the long-term stability. Fig. 5 shows the size distributions of bubble samples that were cooled down to room temperature 200 ms, 1.5 min, and 3 min after their formation at a temperature of 50 °C. The size distributions were measured 1 hour after microbubble formation to allow the bubbles to reach their stable size. Note that the monodispersity decreases for
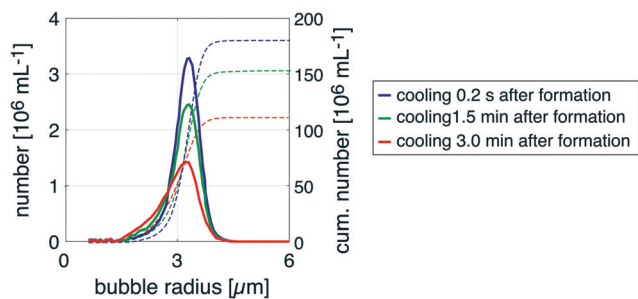
Fig. 5 Size distributions of microbubble samples produced at 50 °C and subsequently cooled down to room temperature 0.2 s, 1.5 min, and 3 min after production. The size distributions were measured 1 h after bubble collection to allow the bubbles to stabilize to their final size.
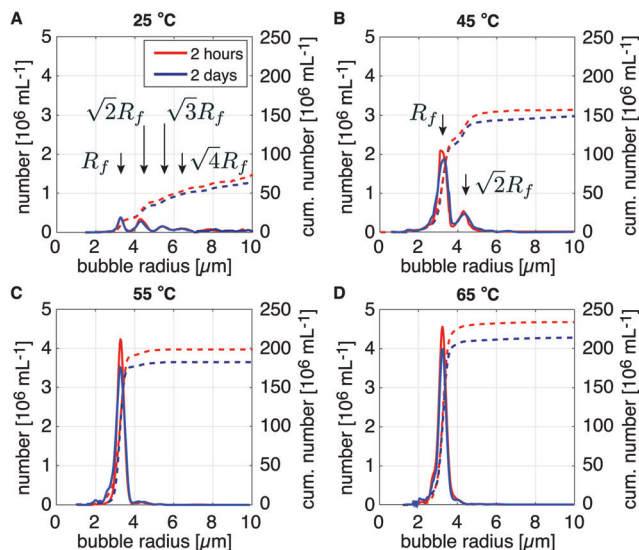

Fig. 6 Size distributions of microbubbles collected in a vial and formed at the same liquid flow-rate and initial bubble radius but, at different temperatures of (A) 25 °C, (B) 45 °C, (C) 55 °C, and (D) 65 °C. The monodispersity and the bubble concentration increase with an increase in the temperature during bubble formation.

increasing times at which the bubbles are maintained at a temperature of 50 °C. Thus, freshly formed bubbles should be cooled to room temperature within a few seconds after their formation to maintain their monodispersity.

A decrease in microbubble stability with temperature has previously been observed for the UCA SonoVue®.[43] The mechanisms by which bubble stability decreases at elevated temperatures are, first, the increased diffusivity of the microbubble filling gas. Second, the decreased rigidity and increased mobility of the lipid molecules potentially leading to buckling of the monolayer and to lipid desorption. Third, the increased area per lipid molecule results in an increased gas permeability of the lipid membrane.[42,44]

The stability of phospholipid molecules in an aqueous dispersion is compromised through, e.g. hydrolization, and the speed of the degradation process increases with temperature.[45,46] However, in the preparation process of the lipid mixtures used for microbubble synthesis by flow-focusing it is common to heat the lipid mixture above the lipid phase transition temperature (>55 °C) for the duration of minutes.[23,24,26] In the experiments performed in this work, the lipid mixture is located within the thermostatic bath for less than 30 seconds. Therefore, the physico-chemical stability of the phospholipid molecules is most certainly not compromised during microbubble formation at elevated temperatures in a flow-focusing device.

3.3 Microbubble stability in the collection vial as a function of the bubble formation temperature

The effect of temperature during bubble formation on the long-term size- and concentration stability of bubble samples collected in vials with a SF_6 headspace was investigated. Fig. 6A–D show the size distributions of bubbles formed at temperatures of 25 °C, 45 °C, 55 °C, and 65 °C, respectively. The size distributions were measured 2 hours (solid red curves) and 2 days (solid blue curves) after bubble formation at an initial on-chip bubble radius R_i of 7.0 ± 0.3 μm using the DSPC based lipid mixture. The cumulative bubble concentration per mL is represented by the dotted lines in

Fig. 6A–D. Note that the monodispersity of the bubble suspensions increases with the temperature during bubble formation. Also note the distinct maxima in the measured bubble number in Fig. 6A and B. The maximum at the smallest bubble radius (at 3.2 μm) corresponds to the final bubble radius R_f of the initially formed on-chip bubble radius of 7 μm, i.e. the ratio R_i/R_f was 2.2, as before. The second- and higher order maxima in the measured bubble number result from the coalescence of two or more bubbles.

Indeed, the position of the higher order maxima in the size distributions can be calculated. Here, it is assumed that the total number of lipid molecules on the surface of a coalesced bubble is the sum of that of the two monodisperse bubbles it originated from. Furthermore, it is known that the surface area of a freshly formed bubble decreases by a factor of $(R_i/R_f)^2$ and that this ratio is independent of R_i.[26,27] Thus, the surface area $A_{f,2}$ of the stable bubble formed due to the coalescence of two monodisperse bubbles is twice the surface area of the stable non-coalesced bubble $A_f = 4\pi R_f^2$. The same argument holds for multiple coalesced bubbles such that $A_{f,n} = nA_f$ and $R_{f,n} = \sqrt{n}R_f$, with n the number of coalesced monodisperse bubbles that form a bigger bubble. The positions of the higher order maxima correspond to the calculated values as indicated in Fig. 6A and B. Thus, indeed, the higher order maxima in the measured bubble number are due to on-chip bubble coalescence.

Note that apart from an increased monodispersity, the cumulative bubble concentration also increased with temperature, see dotted lines in Fig. 6A–D. In a clinical setting, when the transmit frequency of an ultrasound scanner would be tuned to the resonance frequency of the bubbles with radius R_f, then, for the specific case of the bubble sample produced

at a temperature of 25 °C shown in Fig. 6A, only 20 million bubbles per mL would be of a size resonant to the ultrasound driving frequency. However, for the bubble sample produced at 65 °C (Fig. 6D), more than 200 million bubbles per mL will be resonant to the ultrasound driving frequency. Thus, bubble formation using the DSPC based lipid mixture at a temperature of 65 °C resulted in a contrast agent with a 10 times higher sensitivity than that produced at room temperature. Moreover, the echo of the highly monodisperse bubble samples produced at the elevated temperatures have been shown to be more nonlinear than that of a polydisperse agent thereby, *e.g.* enabling deep tissue imaging without shadowing effects.[5]

Finally, note that at all temperatures the produced bubble samples were highly stable over time, *i.e.* the total bubble concentration decreased by only 10–15% over the course of 2 days. No difference in long-term stability can be observed between the bubble samples formed at the different temperatures. Therefore, it can be concluded that bubble formation at elevated temperatures only results in a lower coalescence probability, and, that it does not influence the long-term size- and concentration stability of the bubble suspensions once they have been collected in a vial filled with a SF$_6$ gas headspace.

3.4 Long-term stability in the vial: DPPC *versus* DSPC coated bubbles

The long-term size- and concentration stability of a microbubble suspension formed using the DPPC based lipid mixture was compared to that of a bubble suspension formed using the DSPC based mixture, see Fig. 7A and B, respectively. For both bubble suspensions, the temperature during bubble formation was 60 °C. The size distributions were measured 2 hours, 2 days, 4 days, and 7 days after bubble collection in vials with a SF$_6$ gas-filled headspace. The cumulative bubble concentration is represented by the dotted lines in Fig. 7A and B.
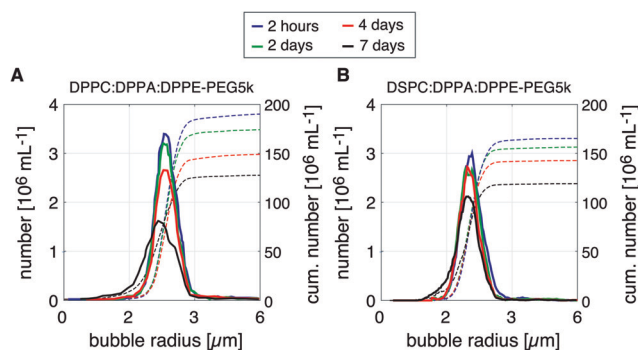
Fig. 7 Long-term size- and concentration stability of a bubble suspensions collected in a vial and formed using (A) a mixture of DPPC:DPPA:DPPE-PEG5000 lipids and (B) using a mixture of DSPC:DPPA:DPPE-PEG5000 lipids. The size distributions were measured 2 hours, 2 days, 4 days, and 7 days after bubble production.

Note that the bubbles formed using the DPPC based lipid mixture were slightly less stable than those formed using the DSPC based mixture. Four days after bubble production, the bubble concentration of the DPPC coated bubbles had decreased by 21% as compared to a decrease of 12% for the DSPC coated bubbles. Seven days after bubble formation, the size distributions of the DPPC and DSPC coated bubbles became wider and shifted towards smaller bubble radii indicating bubble dissolution. Nevertheless, both lipid mixtures resulted in a highly stable bubble suspension for at least two days after their production, both in terms of size- and concentration stability. The time window of 2 to 4 days is sufficiently long for direct *in vivo* injection, or for further processing.

It has been shown before that microbubble stability against dissolution increases with acyl chain length through an increase of the resistive barrier against gas dissolution, which explains the higher stability of the DSPC coated bubbles.[44,47] The stability of the microbubble suspensions produced in this work may be further improved through the use of a microbubble filling gas with a higher molecular weight and a lower aqueous solubility and diffusivity, *e.g.* C$_3$F$_8$ or C$_4$F$_{10}$.[2,48]

Finally, it is of interest to discuss the clinical relevance of the microfluidically synthesized bubble suspensions. The total bubble concentration of the bubble samples (150–250 million bubbles per mL) was similar to the bubble concentration of the clinically available UCA SonoVue® (300 million bubbles per mL). The recommended clinical dose for *in vivo* injection in human consists of 2.4 mL of SonoVue® and contains approx. 700 million bubbles. The microfluidic production of 2.4 mL of microbubble suspension using the flow-focusing device employed in this work takes at least 1 hour. The production time may be decreased through the use of a different flow-focusing geometry[49] and through parallelization.[50,51] However, recently, it has been shown that the sensitivity of a monodisperse bubble suspension is 2 to 3 orders of magnitude higher than that of a polydisperse suspension with the same bubble concentration.[5] Therefore, the injected dose of a monodisperse bubble suspension driven at resonance can be decreased by 2 to 3 orders of magnitude with respect to that of SonoVue® to achieve the same contrast enhancement. Thus, a clinically relevant dose of monodisperse microbubbles can be produced in less than a minute. Furthermore, the total amount of lipids in such a clinically relevant dose of monodisperse bubbles (0.1–0.3 mg) is approximately equal to that in a recommended SonoVue dose (0.2 mg). All in all, this demonstrates the high clinical potential of microfluidically formed monodisperse microbubbles.

4 Conclusions

The coalescence probability of monodisperse phospholipid-coated microbubbles in the outlet of a flow-focusing device can be dramatically reduced by increasing the temperature

during bubble formation. The relative viscosity of the liquid in the thin film between the colliding bubbles increases exponentially with temperature. Furthermore, it was shown that the relative viscosity of a DPPC based lipid mixture is 7.6 times higher than that of a DSPC based lipid mixture at the same total lipid concentration. Therefore, the coalescence probability of bubbles formed using a DSPC based mixture is higher than that of bubbles formed using a DPPC based lipid mixture. The higher relative viscosity of the DPPC based mixture can be explained solely from its 7.6 times higher liposome concentration showing that the relative viscosity is dependent on the liposome concentration and not on the employed primary phospholipid. The results show that the temperature dependent coalescence probability can be predicted by a universal power law of fully independent variables. Furthermore, the ratio of the initial on-chip bubble size to the final stable bubble size was always found to be 2.2 for DPPC:DPPA:DPPE-PEG5000 and for DSPC:DPPA:DPPE-PEG5000 lipid mixtures with 10 mol% PEG, independent of the temperature at which the bubbles were formed. Furthermore, it was shown that the monodispersity of microbubble suspensions formed by flow-focusing at temperatures higher than room temperature is best maintained when the bubbles are rapidly cooled down to room temperature, within seconds after their formation. Moreover, it was demonstrated that microbubble suspensions formed at elevated temperatures are highly stable over a time window of 2 to 4 days with clinically relevant bubble concentrations when collected in a vial with a SF_6 headspace. All in all, this work shows that the efficiency of the use of phospholipids in microbubble formation by flow-focusing can be increased by 5 times through an increase of the temperature at which the bubbles are formed from room temperature to 70 °C.

Conflicts of interest

There are no conflicts to declare.

Acknowledgements

Notes and references

1   J. R. Lindner, *Nat. Rev. Drug Discovery*, 2004, **3**, 527–533.
2   T. Segers, N. de Jong, D. Lohse and M. Versluis, Microbubbles for medical applications, *RSC Nanosci. Nanotechnol.*, 2015, **36**, 81–101.
3   T. G. Leighton, *The Acoustic Bubble*, Academic Press, 1994.
4   A. L. Klibanov, *Invest. Radiol.*, 2006, **41**, 354–362.
5   T. Segers, P. Kruizinga, M. Kok, G. Lajoinie, N. de Jong and M. Versluis, *Ultrasound Med. Biol.*, 2018, **44**(7), 1482–1492.
6   J. M. Tsutsui, F. Xie and R. T. Porter, *Cardiovasc. Ultrasound.*, 2004, **2**, 23.
7   S. Hernot and A. L. Klibanov, *Adv. Drug Delivery Rev.*, 2008, **60**, 1153–1166.
8   L. E. Deelman, A. E. Declèves, J. J. Rychak and K. Sharma, *Adv. Drug Delivery Rev.*, 2010, **62**, 1369–1377.
9   A. R. Carson, C. F. McTiernan, L. Lavery, M. Grata, X. Leng, J. Wang, X. Chen and F. S. Villanueva, *Cancer Res.*, 2012, **72**, 6191–6199.
10 H. Dewitte, K. Vanderperren, H. Haers, E. Stock, L. Duchateau, M. Hesta, J. H. Saunders, S. C. De Smedt and I. Lentacker, *Theranostics*, 2015, **5**, 97–109.
11 T. Segers, N. de Jong and M. Versluis, *J. Acoust. Soc. Am.*, 2016, **140**, 2506–2517.
12 D. E. Goertz, N. de Jong and A. F. W. van der Steen, *Ultrasound Med. Biol.*, 2007, **33**, 1376–1388.
13 M. Emmer, H. J. Vos, D. E. Goertz, A. van Wamel, M. Versluis and N. de Jong, *Ultrasound Med. Biol.*, 2009, **35**, 102–111.
14 J. A. Feshitan, C. C. Chen, J. J. Kwan and M. A. Borden, *J. Colloid Interface Sci.*, 2009, **329**, 316–324.
15 M. P. Kok, T. Segers and M. Versluis, *Lab Chip*, 2015, **15**, 3716–3722.
16 T. Segers and M. Versluis, *Lab Chip*, 2014, **14**, 1705–1714.
17 S. A. Peyman, R. H. Abou-Saleh, J. R. McLaughlan, N. Ingram, B. R. G. Johnson, K. Critchley, S. Freear, J. A. Evans, A. F. Markham, P. L. Coletta and S. D. Evans, *Lab Chip*, 2012, **12**, 4544–4552.
18 A. M. Gañán-Calvo and J. M. Gordillo, *Phys. Rev. Lett.*, 2001, **87**, 274501.
19 S. L. Anna, N. Bontoux and H. A. Stone, *Appl. Phys. Lett.*, 2003, **82**, 364–366.
20 P. Garstecki, H. A. Stone and G. M. Whitesides, *Phys. Rev. Lett.*, 2005, **94**, 164501.
21 A. Churchman, V. Mico, J. de Pablo, S. Peyman, S. Freear and S. Evans, *Microsyst. Nanoeng.*, 2018, **4**, 17087.
22 D. Das, K. Sivasubramanian, C. Yang and M. Pramanik, *Sci. Rep.*, 2018, **8**, 6401.
23 K. Hettiarachchi, E. Talu, M. L. Longo, P. A. Dayton and A. P. Lee, *Lab Chip*, 2007, **7**, 463–468.
24 E. Talu, R. L. Powell, M. L. Longo and P. A. Dayton, *Ultrasound Med. Biol.*, 2008, **34**, 1182–1185.
25 R. Shih and A. P. Lee, *Langmuir*, 2016, **32**, 1939–1946.
26 T. Segers, L. de Rond, N. de Jong, M. Borden and M. Versluis, *Langmuir*, 2016, **32**, 3937–3944.
27 T. Segers, D. Lohse, M. Versluis and P. Frinking, *Langmuir*, 2017, **33**, 10329–10339.
28 J. N. Israelachvili, *Intermolecular and Surface Forces*, Academic Press, 1992, vol. 2.
29 J. Lee, H. Lee and J. Andrade, *Prog. Polym. Sci.*, 1995, **20**, 1043–1079.
30 K. Danov, *Fluid Mechanics of Surfactant and Polymer Solutions*, Springer-Verlag Wien, 2004, ch. 1.
31 H. Barnes, J. Hutton and F. Walters, *An introduction to rheology*, Elsevier, Amsterdam, 1989, vol. 3.
32 D. Trokhymchuk, A. Henderson, A. Nikolov and D. Wasan, *Langmuir*, 2001, **17**, 4940–4947.
33 D. C. Duffy, J. C. McDonald, O. J. A. Schueller and G. M. Whitesides, *Anal. Chem.*, 1998, **70**, 211–217.

34 M. L. F. Nascimentoa and C. Apariciob, *Phys. B*, 2007, **398**, 71–77.

35 M. M. Lozano and M. L. Longo, *Soft Matter*, 2009, **5**, 1822–1834.

36 S. Lee, D. H. Kim and D. Needham, *Langmuir*, 2001, **17**, 5544–5550.

37 F. Olson, C. Hunt, F. Szoka, W. Vail and D. Papahadjopoulos, *Biochim. Biophys. Acta, Biomembr.*, 1979, **557**, 9–23.

38 C. Allen, N. Dos Santos, R. Gallagher, G. Chiu, Y. Shu, W. Li, S. Johnstone, A. Janoff, L. Mayer, M. Webb and M. Bally, *Biosci. Rep.*, 2002, **22**, 225–250.

39 J. Griesbauer, H. Seeger, A. Wixforth and M. F. Schneider, *Method for the Monte Carlo Simulation of Lipid Monolayers including Lipid Movement*, 2010, arXiv, https://arxiv.org/pdf/1012.4973.pdf.

40 E. Boek, J. Padding, W. den Otter and W. Briels, *J. Phys. Chem. B*, 2005, **109**, 19851–19858.

41 D. Bardin, T. Martz, P. Sheeran, R. Shih, P. Dayton and A. Lee, *Lab Chip*, 2011, **23**, 3990–3998.

42 M. Borden, G. Pu, G. Runner and M. Longo, *Colloids Surf., B*, 2004, **34**, 209–223.

43 H. Mulvana, E. Stride, J. Hajnal and R. Eckersley, *Ultrasound Med. Biol.*, 2010, **36**, 925–934.

44 M. Borden and M. Longo, *Langmuir*, 2002, **18**, 9225–9233.

45 H. Frøksjaer, J. Bentz and F. Szoka, in *Optimization of Drug Delivery*, ed. H. Bundgaard, A. Bagger Hansen and H. Kofod, Munksgaard, Copenhagen, 1982, ch. Stability and storage of liposomes.

46 M. Grit, J. de Smidt, A. Struijke and D. Crommelin, *Int. J. Pharm.*, 1989, **50**, 1–6.

47 M. M. Lozano and M. L. Longo, *Langmuir*, 2009, **25**, 3705–3712.

48 K. Sarkar, A. Katiyar and P. Jain, *Ultrasound Med. Biol.*, 2009, **35**, 1385–1396.

49 E. Castro-Hernández, W. van Hoeve, D. Lohse and J. Gordillo, *Lab Chip*, 2011, **11**, 2023–2029.

50 M. Hashimoto, S. S. Shevkoplyas, B. Zasońska, T. Szymborski, P. Garstecki and G. Whitesides, *Small*, 2008, **4**, 1795–1805.

51 E. Amstad, X. Chen, M. Eggersdorfer, N. Cohen, T. Kodger, C. Ren and D. Weitz, *Phys. Rev. E*, 2017, **95**, 043105.